ORIGINAL PAPER

A novel 3D non-degenerate hyperchaotic map with ultra-wide parameter range and coexisting attractors periodic switching

Lilian Huang · **Chuang Li** · **Jin Liu** · **Yu Zhong** ·
Hao Zhang

Abstract Based on trigonometric functions, we propose a three-dimensional (3D) hyperchaotic map with a concise symmetric structure. From the perspective of Lyapunov exponents, we establish the mathematical proof that the new map consistently maintains a chaotic state across an infinitely wide parameter range. Numerical simulations illuminate a diverse array of dynamic behaviors, including an ultra-wide range of non-degenerate hyperchaotic parameters, antimonotonicity, transient chaos, and multiple coexisting attractors. Particularly noteworthy, altering initial values enables the periodic switch of symmetric attractors—a rare phenomenon within other chaotic maps. Moreover, in conjunction with an offset constant, successful polarity transformation of attractors in a single direction has been achieved. Furthermore, performance analysis underscores that the sequence generated by the new map embodies significantly elevated complexity and pseudo-randomness. Finally, we implement the new map using a digital signal processing platform and successfully validate its physical feasibility by obtaining the chaotic attractors.

Keywords Discrete map · Non-degenerate hyperchaotic · Infinitely wide parameter range · Attractors periodic switching · DSP implementation

L. Huang (✉) · C. Li · J. Liu
College of Information and Communication Engineering, Harbin
Engineering University, Harbin 150001, China
e-mail: lilian_huang@163.com

L. Huang · C. Li · J. Liu
MIIT Key Laboratory of Advanced Marine Communication and
Information Technology, Harbin 150001, China

L. Huang
National Key Laboratory of Underwater Acoustic Technology,
Harbin Engineering University, Harbin 150001, China

Y. Zhong · H. Zhang
Southwest China Institute of Electronics Technology, Chengdu
310036, China

1 Introduction

Chaos is a complex dynamic behavior of a deterministic nonlinear system under certain conditions [1]. Due to the properties of the initial sensitivity, internal randomness, and unpredictability, chaotic systems are widely used in secure communication, image encryption, and pseudo-random sequence generation [2–4]. Hyperchaos is a much more complex behavior than chaos since it has more than one positive LE. Therefore, applications based on hyperchaotic systems have a higher security level than those based on general chaotic systems [5]. Generally speaking, to generate hyperchaos, the system dimensions required for a discrete system are lower than the continuous system, which means the applications based on the discrete hyperchaotic system usually have higher computational efficiency and lower resource cost [6,7].

However, when a chaotic system is implemented on hardware with poor computational precision, unpredictable quantization errors are inevitably added in

each iteration, causing the chaotic trajectory to deviate from the initial trajectory. The variables of the iterative state will eventually converge to a periodic cycle over time. Additionally, initial value sensitivity, long-term unpredictability, and ergodicity will all diminish or even vanish [8–10]. In an effort to prevent the dynamic degradation of digital chaos, several efficient anti-degradation techniques, including the perturbation approach, cascade method, analog-digital mixing method, and random jump method, were proposed to improve the dynamic properties of chaotic maps [11–15]. Nevertheless, compared with the original chaotic systems, the improved chaotic systems by the anti-degradation method are also difficult to show advantages in key space, cycle length, sequence complexity, etc. The non-degenerate hyperchaotic system refers to a class of chaotic systems in which the number of positive LEs can reach the maximum possible number. Consequently, their dynamic behaviors are much more complex than the same or lower-dimensional degenerate chaotic system. Additionally, the non-degenerate hyperchaotic system outperforms the degenerate chaotic system in terms of preventing dynamic degradation when the discrete chaotic system is naturally implemented by the digital circuit[7,16,17]. Therefore, the modeling, analysis, and implementation of non-degenerate chaotic systems is a research topic of great theoretical significance and engineering application value.

In recent years, chaotic systems have evolved from low-dimensional systems to complex high-dimensional systems. To generate hyperchaotic systems with better performance, many researchers choose to couple memristors into existing chaotic systems, several chaotic systems that highly sensitive to initial values have been designed and thoroughly studied [18–21]. For instance, in [19], a distinctive memristor-coupled approach reveals intricate coexisting and synchronous behaviors in memristive systems, showcasing diverse attractors and synchronization patterns. In addition, many new construction methods for the non-degenerate hyperchaotic system have also been proposed. Shen et al. [22] proposed a new method for designing ideal dissipative hyperchaotic systems based on the anti-control principle. Reference [23] presented a systematic method for generating continuous-time autonomous hyperchaotic systems with an arbitrary expected positive LE. Reference [24] used a block diagonal matrix in the design of the nominal system

to construct the desired non-degenerate hyperchaotic system. These constructed chaotic systems exhibit rich dynamic behaviors and extremely hidden multistability, contributing to the enhanced security of cryptographic algorithms based on these systems. Nonetheless, certain significant defects, such as a limited parameter range and a discontinuous chaotic domain, still persist in most high-dimensional chaotic systems. On the other hand, although these above studies on non-degenerate hyperchaotic systems can make the number of positive LEs reach the maximum possible number if the configuration method is reasonable, most of these methods are aimed at continuous systems, and the design process is fussy. The complicated structures of those systems usually result in lower computational efficiency and higher resource costs in practical engineering applications.

Based on the above considerations, we aim to propose a high-dimensional non-degenerate hyperchaotic map with a concise structure, an ultra-wide continuous chaotic domain, the largest possible chaotic parameter space, and complex dynamical behavior. To this end, we introduce the sine function into a simple linear map, due to the periodic feedback of the trigonometric function, a new 3D non-degenerate hyperchaotic map is proposed. Our research methodology in this work is consistent with the majority of previous studies on discrete chaotic maps [6,18–23,25], which can be summarized in the following three aspects: chaos theory analysis, numerical simulation, and hardware circuit experiments. Not only does it analyze the complex dynamic characteristics of the new map, but it also demonstrates the physical feasibility of the new map and the applicability of the generated sequences. The novelty of our work can be briefly summarized as follows:

1. The new map simultaneously combines complex dynamic characteristics and a simple kinetic equation. This concise symmetric structure allows for higher computational efficiency and lower resource costs in industrial applications of chaotic systems.
2. The new map exhibits an ultra-wide range of parameters for chaos and non-degenerate hyperchaos. Moreover, it showcases a unique phenomenon of periodic switching between symmetric attractors, which is rarely observed in other maps.
3. The new map can generate two types of coexisting attractors: chaotic attractor and quasi-periodic curve. Within one period of alternating changes
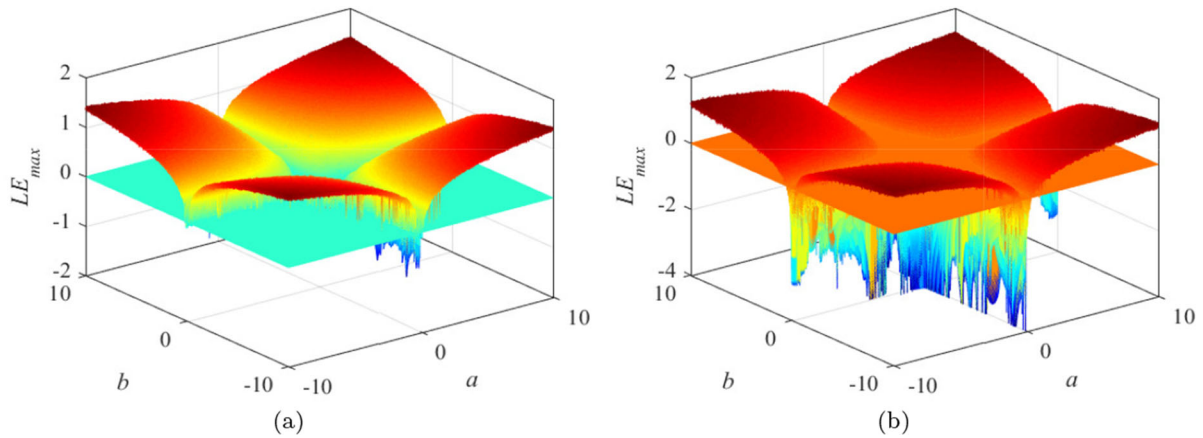
Fig. 1 **a** The $LE_{\max}$ of (1). **b** The $LE_{\min}$ of (1)

between the coexisting attractors, the proportion of each individual attractor varies depending on the initial values.

The rest of this paper is organized as follows: In Sect. 2, a new 3D discrete chaotic map is constructed, and its chaotic parameter range is analyzed and verified. Section 3 analyzes the dynamic behaviors including strange attractors, bifurcation behavior, antimonotonicity, and transient chaos of the new map. Section 4 studies the multistability and the offset-boosting behavior of the new map. In Sect. 5, performance analysis of the sequence generated by the new map and the DSP implementation are conducted. Finally, Sect. 6 summarizes this paper.

2 Construction of a 3D non-degenerate hyperchaotic map

Introducing trigonometric functions into dynamic systems is an effective way to achieve multistability. Inspired by this, a new 3D discrete hyperchaotic map with a concise symmetric structure is constructed. The mathematical model of the new map is written as

$$
\begin{cases}
x_{n+1} = sin(x_n) + asin(y_n) \\
y_{n+1} = sin(y_n) + bz_n \\
z_{n+1} = sin(z_n) + x_n
\end{cases}
\tag{1}
$$

where x_n, y_n, z_n are the state variables of the new map when the number of iterations is n (n is a natural number). a, b are two nonzero system parameters.

2.1 Non-degenerate hyperchaotic region

The LE is one of the most important criteria used to judge whether a system is chaotic in the current chaos research. Generally, the number of positive LEs can be used to directly judge the state of the system. Set the initial values to (0.1, 0.1, 0.1), Fig. 1 show the maximum Lyapunov exponent ($LE_{\max}$) and the minimum Lyapunov exponent ($LE_{\min}$) of the map (1) with the constant change of parameters a and b. It can be observed that the LEs are closely related to the two parameters. Near the two parameters close to 0, there are some periodic and quasi-periodic windows. As the absolute value of the parameters increase, the map (1) gradually enters the chaotic state and finally remains in a continuous non-degenerate hyperchaotic state. Moreover, the value of $LE_{\min}$ is also proportional to the absolute value of the parameters, which makes the map (1) within a large range of parameters, as shown in Fig. 2, all the LEs are positive and show an upward trend in general, which indicates that (1) owns an ultra-wide parameters range of non-degenerate hyperchaotic state, and its chaotic characteristics are also enhanced with the increase of the LEs.

2.2 Infinitely wide parameter range of chaos

To prove that map (1) always maintains the chaotic state with a positive LE across an infinitely wide range of parameters, only the following two criteria need to be met [23]:

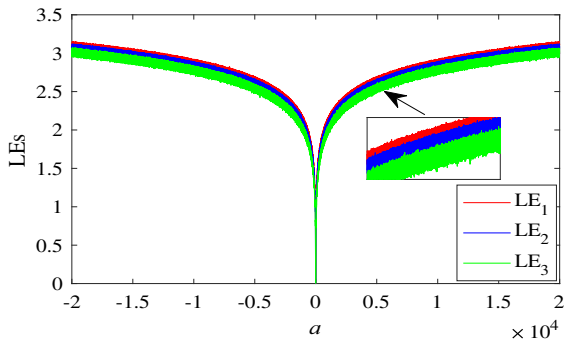1. The trajectory is globally bounded.

Fig. 2 The LEs spectrum when $a \in [-20000, 20000]$

2. Has at least one positive LE.

According to the difference equation of the map (1), the system only contains linear terms and trigonometric function terms. From the boundedness of the trigonometric function, it can be concluded that the state variable x_n of the system is globally bounded since the linear combination of bounded functions and trigonometric functions is still bounded, so we can easily conclude that the other two state variables y_n and z_n of the map (1) are also globally bounded.

To prove that the map (1) has at least one positive LE in an infinitely wide parameter range, massive iterative operations are required to calculate the output sequence when a and b are used as unidentified variables to acquire the analytical solution of the LEs. This method is computationally intensive and almost impossible to complete. Reference [25] proposed a modified perturbation method, which can evaluate the output sequence of the discrete map without replacing concrete parameters.

Here, we introduce the modified perturbation method. Suppose the difference equation of an N-dimensional discrete map is

$$
\begin{cases}
x_1(n+1) = F_1(p, x_1(n), x_2(n), \ldots, x_N(n)) \\
x_2(n+1) = F_2(p, x_1(n), x_2(n), \ldots, x_N(n)) \\
\quad \vdots \\
x_N(n+1) = F_2(p, x_1(n), x_2(n), \ldots, x_N(n))
\end{cases}
\tag{2}
$$

where $x_N(n)$ is the nth$(n \in N^*))$ iteration value of the Nth state variable, $p(p \in R)$ is a control parameter, $F : R^N \to R^N$.

Assign $p = p_0$ as the base point, fix the initial values $[x_1(0), x_2(0), \ldots, x_N(0)]^T$, in this case, there is

no unknown variable in the map (2), and its iteration output matrix of the map (2) is as follows:

$$
H = \begin{bmatrix}
x_1(0) & x_1(1) & \cdots & x_1(n) \\
x_2(0) & x_2(1) & \cdots & x_2(n) \\
\vdots & \vdots & \ddots & \vdots \\
x_j(0) & x_j(1) & \cdots & x_j(n)
\end{bmatrix}
$$

Set $p_1 = p_0 + \Delta p$, Δp is a minor increment, now the output matrix can be described as:

$$
H^* = \begin{bmatrix}
x_1(0) & x_1^*(1) & \cdots & x_1^*(n) \\
x_2(0) & x_2^*(1) & \cdots & x_2^*(n) \\
\vdots & \vdots & \ddots & \vdots \\
x_N(0) & x_N^*(1) & \cdots & x_N^*(n)
\end{bmatrix}
$$

To obtain the specific output matrix H^*, typically, parameter p_1 and initial value $[x_1(0), x_2(0), \ldots, x_N(0)]^T$ are substituted into (2) for iteration. Differently, the modified perturbation method is based on the output matrix H, and let $x_N^*(n)$ perform the Taylor series expansion near the base point $p = p_0$, and then yields:

$$
x_N^*(n) = F_N + (p_1 - p_0) F_N' + \cdots
$$
$$
+ \frac{(p_1 - p_0)^n F_N^{(n)}}{n!} + R_n
$$

Based on the demand for calculation accuracy, choose the appropriate location for truncation, and substitute the obtained $x_N^*(n)$ back into the matrix H^*, the output matrix at the parameter p_1 can then be obtained.

The modified perturbation method uses the perturbation increment to calculate the output sequence under different parameters and then calculates the LEs. As a result, it obviates the need for extensive iterative operations on the substitution equation and allows obtaining the output sequence of the equation with little loss of accuracy.

For the map (1), since parameter a only appears in the expression of x_{n+1} and is a one-order term, so we can regard $x_{n+1} = F_1(a, x_n, y_n, z_n)$ as a first-order function of a, and the impact of a on y_{n+1} and z_{n+1} is ignored here. Therefore, we can cast off the limitation that Δp can only take a minor increment when carrying out the Taylor series expansion.

Fix parameter $b = 10$ and initial values $(1, 1, 1)$. Set the base point $a_0 = 10$, when $a_i = a_0 + i, (i \in N^*)$, i is the perturbation increment, the output matrix of (1)

Table 1 The LEs calculated by two methods

Parameter	Traditional method	Perturbation method
$a=11$	1.4209,1.3537,1.2449	1.4141,1.3467,1.2252
$a=10^3$	2.8853,2.8470,2.7847	2.8798,2.8400,2.7759
$a=10^5$	4.4112,4.3847,4.3447	4.4003,4.3722,4.3284
$a=10^7$	5.9389,5.9148,5.8803	5.9276,5.9070,5.8714

is as follows:

$$\begin{bmatrix} x_0 & x_1 + i\sin(y_1) & \cdots & x_n + i\sin(y_n) \\ y_0 & y_1 & \cdots & y_n \\ z_0 & z_1 & \cdots & z_n \end{bmatrix}$$

Table 1 lists the results that acquired by the modified perturbation method and the traditional method. As can be seen that the LEs calculated by the modified perturbation method are very close to those calculated by the traditional method (the number of iterations is 10^5). Next, this paper will use the modified perturbation method to prove that the map (1) has at least one positive LE within an infinitely wide parameter range.

The definition method of calculating the LE is given by

$$\text{LE} = \lim_{\substack{n \to \infty \\ \varepsilon \to 0}} \frac{1}{n} \ln \left| \frac{F^n(x_0 + \varepsilon) - F^n(x_0)}{\varepsilon} \right| \tag{3}$$

where $F^n(x_0)$ denotes the value iterated n times at the initial value x_0.

Take parameter a as an example, set $b = 10$ and the initial values (1, 1, 1). Assign the base point $a_0 = 10$, $a_i = a_0 + i (i \in N^*)$, where i is the perturbation increment. Take $a_0 = 10$, the LEs calculated by QR orthogonal decomposition method are $LE_1^0 = 1.384$, $LE_2^0 = 1.315$, $LE_3^0 = 1.192$. When applying the modified perturbation method to calculate the LEs, set two groups of initial values as $[x_0, y_0, z_0]$, $[x_0 + \varepsilon, y_0, z_0]$ (ε is an infinitesimal quantity), respectively, and the output matrix under the two groups of initial values can be expressed as:

$$\begin{bmatrix} x_0 & x_1 & \cdots & x_n \\ y_0 & y_1 & \cdots & y_n \\ z_0 & z_1 & \cdots & z_n \end{bmatrix}, \begin{bmatrix} x_0 + \varepsilon & x_1^* & \cdots & x_n^* \\ y_0 & y_1^* & \cdots & y_n^* \\ z_0 & z_1^* & \cdots & z_n^* \end{bmatrix}$$

From (2) and $LE_1^0 = 1.384$, one obtains:

$$LE_1^0 = \lim_{\substack{n \to \infty \\ \varepsilon \to 0}} \frac{1}{n} \ln \left| \frac{x_n^* - x_n}{\varepsilon} \right| > 0 \tag{4}$$

Let $S_1 = \frac{x_n^* - x_n}{\varepsilon}$, then

$$|S_1| > 1 \tag{5}$$

Next, we will prove that map (1) has at least one positive LE in an infinitely wide range of parameter by mathematical induction, and prove that this positive LE is proportional to the change of parameter a.

(1) When $i = 1$, $a_1 = a_0 + i = 11$, all the LEs of the map (1) are calculated as $LE_1^1 = 1.421$, $LE_2^1 = 1.354$, $LE_3^1 = 1.245$, on this condition, the map (1) has three positive LEs, and $LE_1^1 > LE_1^0$. The output matrices of the map (1) under two groups of initial values when applying the perturbation method are acquired as follows:

$$\begin{bmatrix} x_0 & x_1 + i\sin(y_1) & \cdots & x_n + i\sin(y_n) \\ y_0 & y_1 & \cdots & y_n \\ z_0 & z_1 & \cdots & z_n \end{bmatrix},$$

$$\begin{bmatrix} x_0 + \varepsilon & x_1^* + i\sin(y_1^*) & \cdots & x_n^* + i\sin(y_n^*) \\ y_0 & y_1^* & \cdots & y_n^* \\ z_0 & z_1^* & \cdots & z_n^* \end{bmatrix}$$

From (2), one of the LEs is calculated as:

$$LE_1^1 = \lim_{\substack{n \to \infty \\ \varepsilon \to 0}} \frac{1}{n} \ln \left| S_1 + \frac{\sin(y_n^*) - \sin(y_n)}{\varepsilon}) \right| > 0 \tag{6}$$

Let $S_2 = \frac{\sin(y_n^*) - \sin(y_n)}{\varepsilon}$, then we can obtain:

$$|S_1 + S_2| > 1, |S_1 + S_2| > |S_1| \tag{7}$$

(2) Suppose when $i = m$, the proposition is true, that is, when $a_m = a_0 + m$, there is

$$LE_1^m > 0, LE_1^m \geq LE_1^{m-1} \tag{8}$$

Now, the output matrix of (1) under two groups of initial values are as follows:

$$\begin{bmatrix} x_0 & x_1 + m\sin(y_1) & \cdots & x_n + m\sin(y_n) \\ y_0 & y_1 & \cdots & y_n \\ z_0 & z_1 & \cdots & z_n \end{bmatrix},$$

$$\begin{bmatrix} x_0 + \varepsilon & x_1{}^* + m\sin(y_1{}^*) & \cdots & x_n{}^* + m\sin(y_n{}^*) \\ y_0 & y_1{}^* & \cdots & y_n{}^* \\ z_0 & z_1{}^* & \cdots & z_n{}^* \end{bmatrix}$$

$$LE_1^m = \lim_{\substack{n \to \infty \\ \varepsilon \to 0}} \frac{1}{n} \ln |S_1 + mS_2| > 0 \qquad (9)$$

thus, one gets:

$$|S_1 + mS_2| > 1, |S_1 + mS_2| > |S_1 + (m-1)S_2| \qquad (10)$$

(3) When $i = m + 1$, the output matrix of (1) under two groups of initial values are as follows:

$$\begin{bmatrix} x_0 & x_1 + (m+1)\sin(y_1) & \cdots & x_n + (m+1)\sin(y_n) \\ y_0 & y_1 & \cdots & y_n \\ z_0 & z_1 & \cdots & z_n \end{bmatrix},$$

$$\begin{bmatrix} x_0 + \varepsilon & x_1{}^* + (m+1)\sin(y_1{}^*) & \cdots & x_n{}^* + (m+1)\sin(y_n{}^*) \\ y_0 & y_1{}^* & \cdots & y_n{}^* \\ z_0 & z_1{}^* & \cdots & z_n{}^* \end{bmatrix}$$

$$LE_1^{m+1} = \lim_{\substack{n \to \infty \\ \varepsilon \to 0}} \frac{1}{n} \ln |S_1 + (m+1)S_2| \qquad (11)$$

When the positive and negative properties of S_1, S_2 are the same, from (10) we can get:

$$|S_1 + (m+1)S_2| > |S_1 + mS_2| > 1 \qquad (12)$$

Namely: $LE_1^{m+1} > LE_1^m > 0$. On this condition, the proposition is true.

When the positive and negative properties of S_1 and S_2 are different, and $|S_2| > 2|S_1|$, obviously, since $|S_1 + S_2|$ and $|S_2|$ have the same positive and negative properties, so $|S_1 + mS_2|$ and $|S_2|$ also have the same positive and negative properties, and because $m > 1, m \in N^*$, then $|S_1 + (m-1)S_2|$ and $|S_2|$ have the same positive and negative properties, From (10), one obtained:

$$|S_1 + mS_2 + S_2| > |S_1 + (m-1)S_2 + S_2| > 1 \qquad (13)$$

Organize and obtain:

$$|S_1 + (m+1)S_2| > |S_1 + mS_2| > 1 \qquad (14)$$

Namely: $LE_1^{m+1} > LE_1^m > 0$. The proposition is proved.

Table 2 The corresponding LEs and states of (1) under several typical parameters settings

(a,b)	(LE_1, LE_2, LE_3)	System state
$(0.5,1)$	$(-0.27, -0.30, -5.25)$	Period-2
$(-1.11,1)$	$(0.05, -0.01, -1.18)$	Quasi-periodic state
$(1.57,1)$	$(0.30, -0.01, -0.55)$	Chaotic
$(-5.2,0.5)$	$(0.16, -0.03, -0.24)$	Chaotic
$(2.37,1)$	$(0.58, 0.14, -0.37)$	Hyperchaotic
$(40,30)$	$(0.65, 0.51, 0.31)$	Non-degenerate hyperchaotic

Similarly, fixed $a = 10$, $b_0 = 10$, set $b_i = b_0 + i$, it can also be obtained that the map (1) has at least one positive LE in such an infinitely wide parameter range. In a conclusion, map (1) has an infinite two-dimensional parameter space $[a, b]$, in which the system can always maintain the chaotic state.

3 Dynamic behaviors

3.1 Strange attractors

Table 2 lists the LEs and corresponding system state of the map (1) under several typical parameters settings, with these settings, Fig. 3 shows the phase diagram of the map (1). As can be seen, there is a big difference in the attractors between different system states, even in the same state, chaotic for example, the trajectory of the map (1) also has great differences. When the map (1) is in the non-degenerate hyperchaotic state, in particular, its attractor becomes a cuboid with strong ergodicity.

3.2 Parameter-relied bifurcation behaviors

To investigate the effects of parameters on the bifurcation behavior and the LEs, fix the initial values as $(0.1, 0.1, 0.1)$. Figure 4 plots the bifurcation diagram of the state variable x_n and the LE spectrum when parameter a changes. It is clearly viewed that the map (1) shows rich dynamic behaviors. Keep $b=1$ while gradually increasing a from 0, the map (1) goes through a short quasi-periodic window after a period-doubling bifurcation, and then enters a chaotic state; as a decreases from 0, the map (1) undergoes transitions among quasi-periodic, periodic, and chaotic states before finally stabilizing into a chaotic state. Additionally, it can be
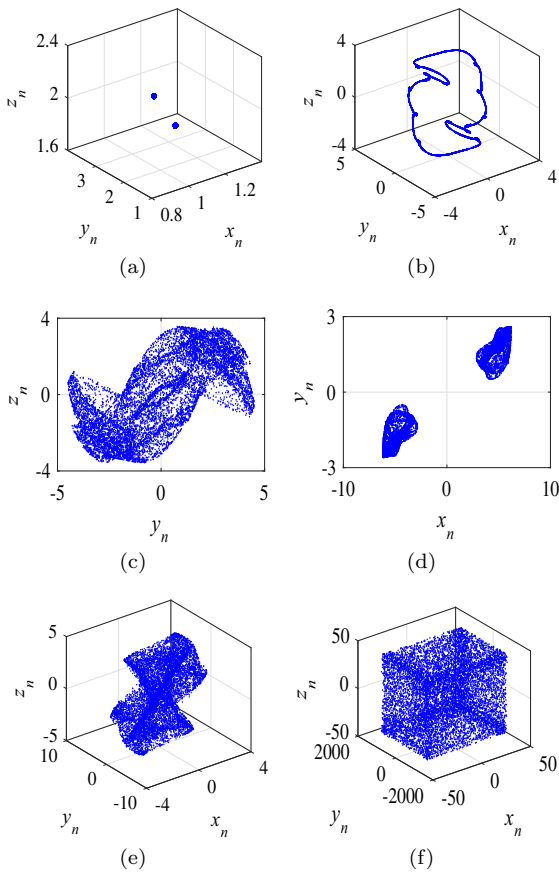
Fig. 3 Phase diagram of attractors under different parameters. **a** Period-2 attractor with discrete points. **b** Quasi-periodic attractor with closed curves. **c** Chaotic attractor. **d** Symmetric chaotic attractor with two pieces. **e** Hyperchaotic attractor. **f** Non-degenerate Hyperchaotic attractor with cuboid structure

observed that the period and quasi-periodic region of the map (1) increase significantly when b is reduced to 0.1. In this case, as a increases from 0, the map (1) owns the route to chaos in the way of period-doubling bifurcation and inverse period-doubling bifurcation; when a decreases from 0, a wide range of period and quasi-period, bifurcation fracture and other special phenomena exist in the map (1). To sum up, the map (1) exhibits complex dynamical behaviors which are highly dependent on the parameters.

3.3 Antimonotonicity

In various nonlinear systems, when a parameter of the system changes monotonically, the periodic orbits generate and disappear by the inverse period-doubling

bifurcation, which is called antimonotonicity [26]. As a fundamental phenomenon in the bifurcations of chaotic systems, it has significant implications for experiments on the fine structure of chaotic systems. Parlitz et al. [27] first reported the antimonotonicity in the Duffing oscillator. Reference [28] pointed out that antimonotonicity is a special property in Chua's circuit. Later, the jerk circuit based on memristor also reported the antimonotonicity phenomenon [29]. In [30,31], antimonotonicity was observed in the logistic map and derived maps from the logistic map. As a discrete system, the map (1) has the property of antimonotonicity. Fix the initial values as (0.1, 0.1, 0.1), and let parameter b take different values. Figure 5 presents the bifurcation diagram of the state variable x_n with the change of the parameter a, in Fig. 5a, a reverse period-doubling bifurcation occurred from period-2 to period-1 at $b = 0.07$, generating a period-2 bubble; when b increases to 0.08, a reverse period-doubling bifurcation from period-4 to period-2, and from period-2 to period-1 occurred as shown in Fig. 5b, and a period-4 bubble was generated in the original period-2 bubble; when b is further increased to 0.09, a small chaotic window appeared in the period-4 bubble as shown in Fig. 5c; when b increases to 0.1, the map exhibits a reverse period-doubling bifurcation from period-2 to period-1, and from period-8 to period-4 as shown in Fig. 5d, simultaneously accompanied by the special bifurcation behavior of bifurcation and fracture.

Hence, it can be concluded that map (1) has rich dynamic behaviors with minor change in parameters, these characteristics also make the application prospect of the map (1) wider. Especially, the critical state between ordered dynamics and chaotic dynamics caused by period-doubling bifurcation makes the discrete chaotic maps have potential application value in reservoir calculation and other research fields [32,33].

3.4 Transient chaos

In nonlinear systems, during a certain transient time, the system trajectory exhibits chaos in a certain region of the phase space and ultimately falls into normal motion, this state transition phenomenon is called transient chaos. For map (1), fixed initial values (0.1, 0.1, 0.1), when parameters are set to $a = 1.715$, $b = 1$, the first 8, 800 iteration points are hyperchaotic state, and then turn to period state. The time series generated by
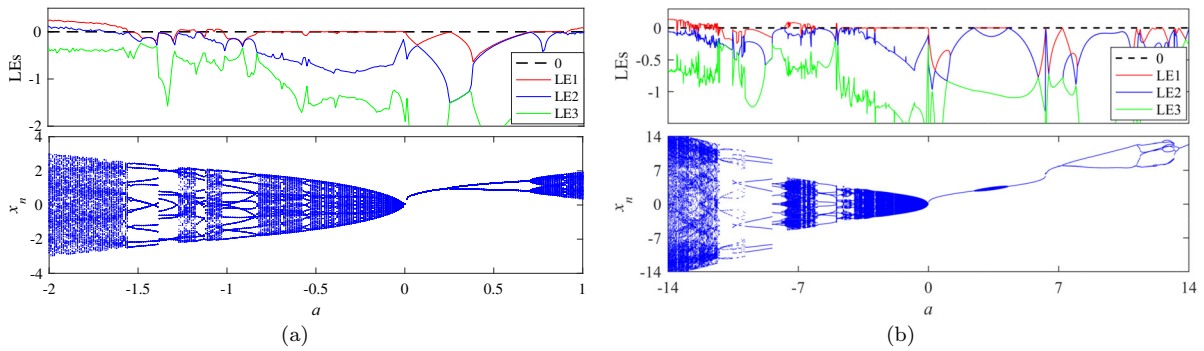
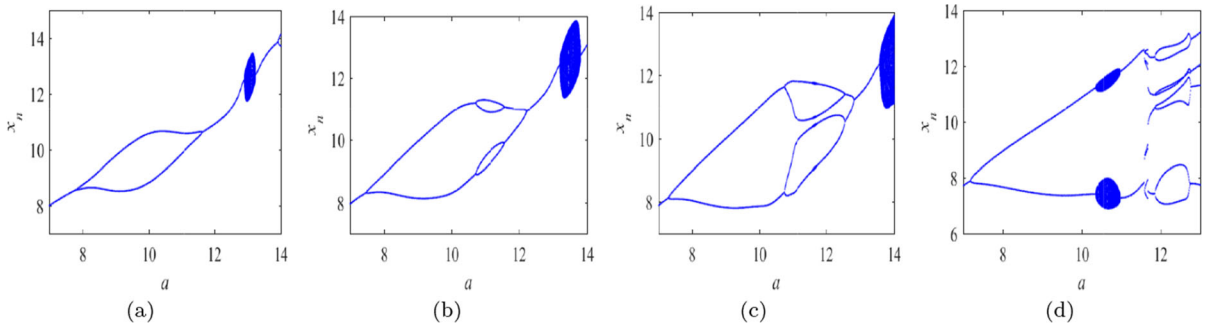**Fig. 4** Bifurcation diagram of x_n and the LEs spectrum. **a** $b=1$. **b** $b=0.1$

Fig. 5 Bifurcation diagrams of x_n with varying a under different parameter b. **a** $b=0.07$. **b** $b=0.08$. **c** $b=0.09$. **d** $b=0.1$
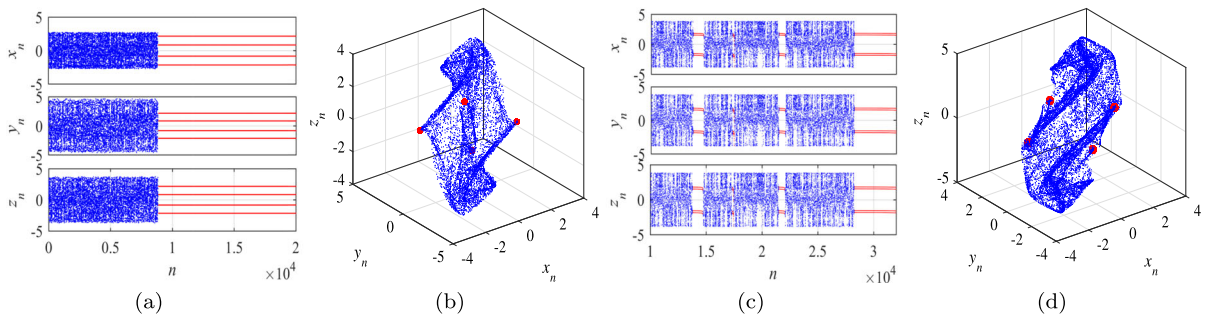

Fig. 6 **a** The sequences diagram when $a = 1.715, b = 1$. **b** The phase diagram when $a = 1.715, b = 1$. **c** The sequence diagram when $a = 2.85, b = 0.5$. **d** The phase diagram when $a = 2.85, b = 0.5$

the map (1) and its corresponding phase diagram are shown in Fig. 6a, b. When the system parameters are set to $a = 2.85$, $b = 0.5$, the time series generated by the map (1) and its corresponding phase diagram are shown in Fig. 6c, d. It can be seen that the system presents an alternation of transient chaos and period within the number of iterations $n = (10, 000, 32, 000)$. In summary, the map (1) demonstrates state transition phenomena such as transient chaos and transient periodicity. Moreover, the choice of iteration values allows

for the generation of multiple states, thereby significantly increasing the complexity of map (1).

4 Multistability and offset boosting

4.1 Coexisting attractors

Multistability refers to the phenomenon that, when the parameter of a nonlinear dynamic system is fixed, the
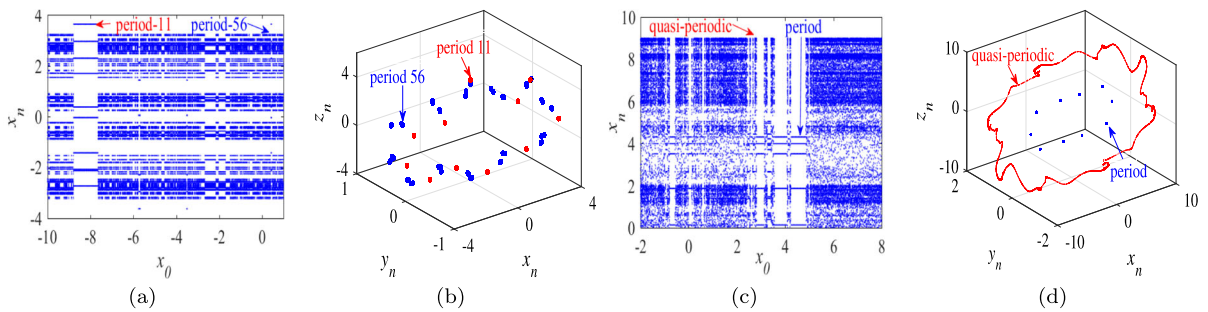
Fig. 7 **a** Bifurcation diagram when $a = -4.5, b = 0.1$. **b** Coexisting periodic attractors, blue: $(0.1, 0.1, 0.1)$, red: $(-8, 0.1, 1)$. **c** Bifurcation diagram when $a = -8$, $b = 0.1$. **d** Coexisting periodic attractor and quasi-periodic curve, blue: $(0.1, 0.1, 0.1)$, red: $(5.5, 0.1, 1)$. (Color figure online)

trajectory of the nonlinear dynamic system is changed by changing the initial conditions of the state variables, resulting in different types of coexisting attractors. If the topological structure and spatial position of the coexisting attractors show a completely symmetric form, it is called symmetric coexisting attractors. The map (1) constructed in this paper also has the multistability with the coexistence of multiple states. Fix initial values $y_0 = z_0 = 0.1$. When the system parameters are set to $a = -4.5$, $b = 0.1$, the bifurcation diagram of x_n for varying x_0 is shown in Fig. 7a, as can be seen that with the change of x_0, there are many coexisting periodic states in the map (1), the coexisting periodic phase diagram under two sets of initial values $(0.1, 0.1, 0.1)$ and $(-8, 0.1, 0.1)$ is shown in Fig. 7b. When the system parameters are set to $a = -8$, $b = 0.1$, the bifurcation diagram of x_n when x_0 changes is shown in Fig. 7c, the coexistence of periodic point and quasi-periodic curve under two sets of initial values $(0.1, 0.1, 0.1)$ and $(5.5, 0.1, 1)$ are shown in Fig. 7d. When combined with some appropriate controls, this initial dependent multistability can be used to induce explicit switching between different coexisting states, which provides great flexibility for many chaos-based engineering applications.

4.2 Attractors periodic switching

Fix $a = b = 1$, set the initial values $y_0 = 0.3$, $z_0 = 0.1$, the top half of Fig. 8a draws the bifurcation diagram of x_n with varying x_0. As can be seen, the change in the initial value x_0 causes the state variable x_n to periodically change within a range of values with oppo-

site polarities. When x_0 and y_0 change, the attraction basin of (1) is shown in the bottom half of Fig. 8a. Different color regions in the figure represent different types of attractors. Figure 8b plots the phase diagram of coexisting attractors when the initial values are $(0.1, 3, 0.1)$ and $(5.5, 3, 0.1)$, respectively. The color of attractors corresponds to the color of different initial value regions in Fig. 8a. It can be seen that the basin of attraction of (1) appears as the alternation of two color regions, and the topological structure and spatial position of the attractors corresponding to the initial values in these two regions show a completely symmetric form. When y_0 is fixed, with the change of x_0, the map (1) presents a periodic switching of two coexisting symmetric attractors, and the proportion of the two attractors will change with the difference of y_0 within a period of x_0. Besides, when x_0 is fixed, with the gradual change of y_0, the map (1) may maintain one type of attractor without change, or maybe exhibit periodic switching between two coexisting symmetric attractors, which depends on the specific value of x_0. Interestingly, due to the symmetric structure of the map (1), it also generates the symmetric coexisting attractors under two sets of initial values with completely opposite polarity. When the initial values are taken as $(0.1, 3, 0.1)$ and $(-0.1, -3, -0.1)$, respectively, the corresponding phase diagram of attractors is shown in Fig. 8c. As can be seen, the map (1) produces a pair of attractors with the same symmetric structure about the origin, whether it is a periodic change of a single initial value or two sets of initial values with completely opposite polarity. Figure 9a, b, respectively, draw the sequences generated by the map (1) under two sets of initial values. As can be observed, when a single initial
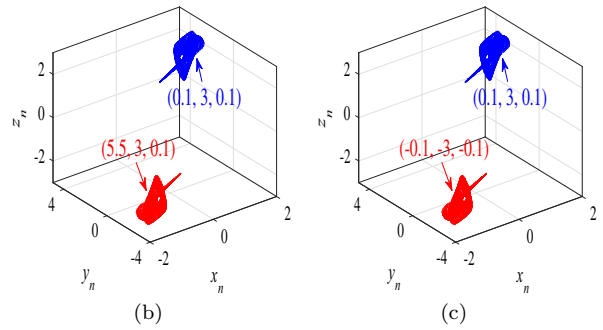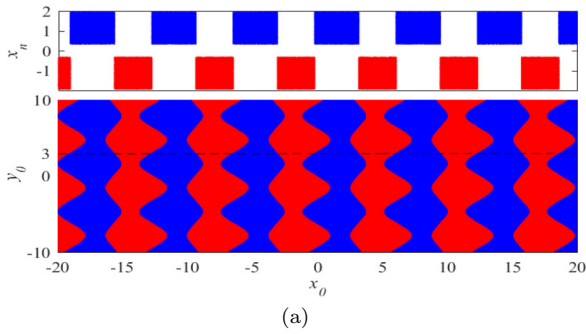
(a)

(b)

(c)

Fig. 8 **a** The bifurcation diagram of x_n with varying x_0 (top) and the attraction basin of (1) with x_0 and y_0 change (bottom). **b** Symmetric coexisting attractors under different initial values, blue: (0.1, 3, 0.1), red:

(5.5, 3, 0.1), red: (0.1, 3, 0.1). **c** Symmetric coexisting attractors under different initial values, blue: $(-0.1, -3, -0.1)$, red: (0.1, 3, 0.1). (Color figure online)
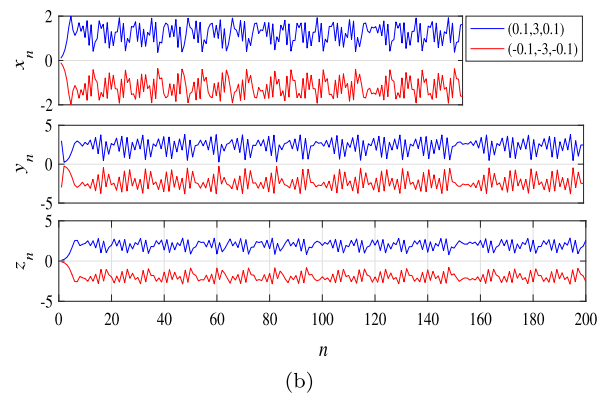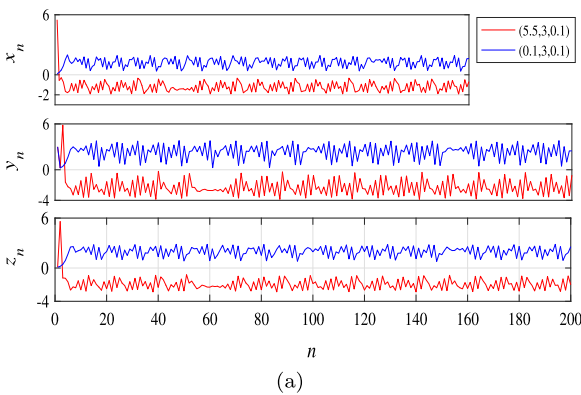

(a)

(b)

Fig. 9 The time sequences of (1) under two sets of initial values. **a** blue: (0.1, 3, 0.1), red: (5.5, 3, 0.1). **b** blue: (0.1, 3, 0.1), red: $(-0.1, -3, -0.1)$. (Color figure online)

value changes, the corresponding time sequences of the two symmetric attractors generated are different, while when the polarity of the initial values is completely opposite, the elements in the two time sequences generated by it are symmetric.

In addition, when fixing $a = 1.5$, $b = 0.5$ and the initial values $y_0 = 3$, $z_0 = 0.1$, the top half of Fig. 10a draws the bifurcation diagram of x_n with varying x_0, as can be seen, changing the initial value x_0 leads to periodic changes in the state variable x_n within a range of values with opposite polarities. Furthermore, when x_0 and y_0 change, the attraction basin of (1) is depicted in the bottom half of Fig. 10a. Figure 10b plots the phase diagram of coexisting quasi-periodic curves when the initial values are (0.1, 3, 0.1) and (5, 3, 0.1), respectively. The color of the initial value area in Fig. 10a corresponds to the color of the quasi-periodic curves. It can also be observed from Fig. 10b that under the

quasi-periodic state, the system can generate two types of quasi-periodic curves with the same topology and symmetrical spatial position. Similar to the two chaotic attractors in Fig. 8b, these two types of quasi-periodic curves exhibit periodic switching or maintain one type without changes as the parameter a varies.

Similarly, the map (1) can also generate symmetric coexisting quasi-periodic curves under two sets of initial values with completely opposite polarity. Fixing the initial values (0.1, 3, 0.1) and $(-0.1, -3, -0.1)$, respectively, the phase diagram is shown in Fig. 10b. Figure 11a, b, respectively, draw the sequences generated by the map (1) under those two sets of initial values. The obtained results lead to the same conclusion as before.

The above results and analysis indicate that map (1) has complex multistability with the coexistence of multiple states; in particular, its symmetric attractors and
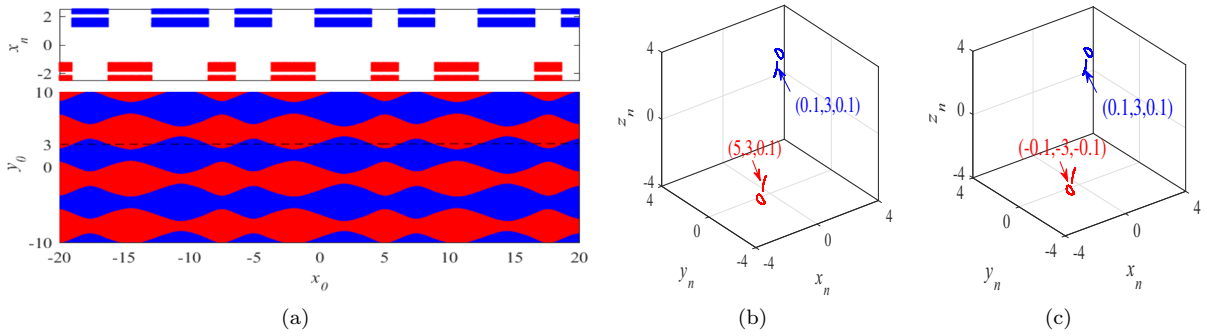
(a)   (b)   (c)

Fig. 10 **a** The bifurcation diagram of x_n with varying x_0 (top) and the attraction basin of (1) with x_0 and y_0 change (bottom). **b** Symmetric coexisting quasi-periodic curves under different initial values, blue: (5, 3, 0.1), red: (0.1, 3, 0.1). **c** Symmetric coexisting quasi-periodic curves under different initial values, blue: $(-0.1, -3, -0.1)$, red: (0.1, 3, 0.1). (Color figure online)
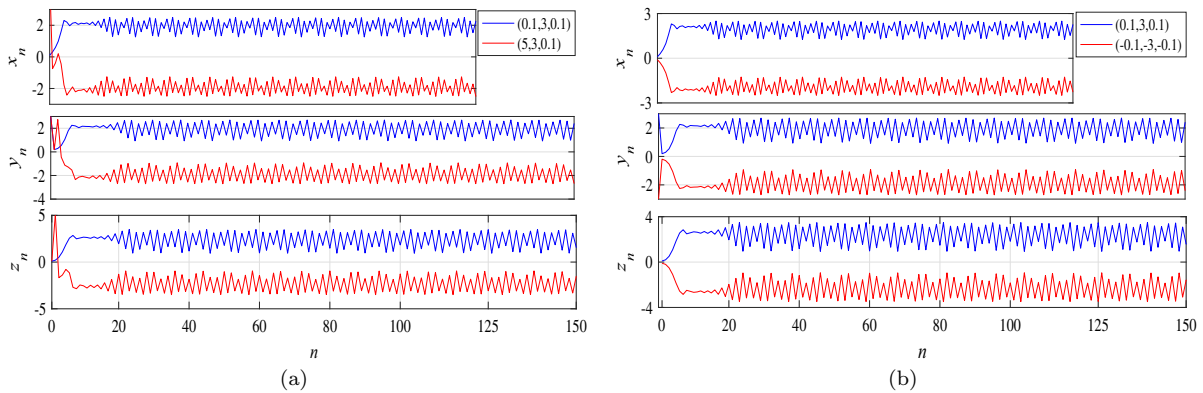

(a)   (b)

Fig. 11 The time sequences of (1) under two sets of initial values. **a** blue: (0.1, 3, 0.1), red: (5, 3, 0.1). **b** blue: (0.1, 3, 0.1), red: $(-0.1, -3, -0.1)$. (Color figure online)

quasi-periodic curves can switch periodically with a single parameter changing. This special property not only greatly enhances the dynamic properties of the map (1), but also brings new directions and possibilities to the control research and engineering applications based on the chaotic sequences.

4.3 Offset boosting

Offset boosting is a displacement phenomenon of chaotic attractors. By changing the offset constant, the spatial position of attractors can be changed, and the topology of attractors before and after the displacement is consistent, thus realizing the mutual conversion between bipolar signals and unipolar signals, so as to meet the demands of chaotic signals in different application fields. In this paper, an offset constant p is

added to the map (1), which is used as a controller of the attractor in the direction of x_n. The map difference equation after adding an offset constant is written as

$$\begin{cases} x_{n+1} = sin(x_n + p) + asiny_n - p \\ y_{n+1} = siny_n + bz_n \\ z_{n+1} = sinz_n + x_n + p \end{cases} \quad (15)$$

Fix initial value (0.1, 0.1, 0.1). When parameter $b = 1$ and $b = 20$, Figs. 12a and 13a, respectively, draw the bifurcation diagram of x_n with varying parameter a when $p = -20, 0, 20, 40$. As can be seen, the variety of p only changes the value range of state variable x_n, but does not change its bifurcation behavior. When parameters $a = -1.11$, $b = 1$, and $a = b = 20$, the attractors of (15) with $p = -20, 0, 20, 40$ are, respectively, shown in Figs. 12b and 13b. We can see that
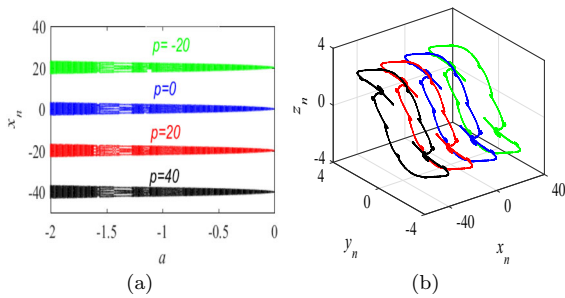
Fig. 12 **a** Bifurcation diagram of x_n. **b** The phase diagram when $p = -20$ (green), 0 (blue), 20 (red), 40 (black). (Color figure online)
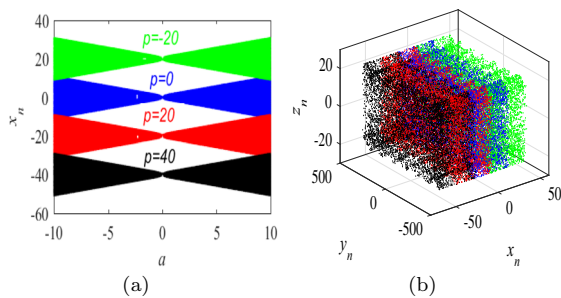

Fig. 13 **a** Bifurcation diagram of x_n. **b** The phase diagram when $p = -20$ (green), 0 (blue), 20 (red), 40 (black). (Color figure online)

with the change of p, the motion track of the state variable x_n moves uniformly, thus achieving the purpose of polarity conversion. Similarly, we can also realize the polarity transformation of the trajectory in the directions of y_n and z_n.

5 Performance analysis and hardware implementation

5.1 Performance of chaotic sequences

For the sequence generated by the map (1), this section will evaluate its performance from the following aspects: the $LEmax$, spectral entropy (SE) [34], permutation entropy (PE) [35], correlation dimension (CorDim) [36] and NIST test. SE is a method of measuring structural complexity, which can be used to measure the complexity of time series generated by any chaotic maps. Here, the SE algorithm represents the complexity of a discrete map by measuring the proximity between the sequence generated by (1) and the random sequence. The larger the SE, the more complex

the sequence. PE is a method for detecting dynamic mutations and the randomness of time series, which can quantitatively evaluate the random noise contained in signal sequences. The size of the arranged entropy value represents the randomness of the sequence: the smaller the entropy value, the simpler and more regular the sequence; on the contrary, the larger the entropy value, the more complex and random the time sequence is. CorDim is a fractal dimension that can measure the dimension of the space occupied by a group of discrete state points. It can be calculated by the Grassberger–Procaccia algorithm [36]. The size of the CorDim value is proportional to the complexity of the map. The larger the CorDim value, the more prominent the dynamic performance of sequences generated by the discrete chaotic map.

Table 3 compares the dynamic performance of the constructed map (1) with the existing classical chaotic maps and the same dimensional chaotic maps in their respective chaotic regions (all chaotic sequences are set to a length of 10^5). These classic chaotic maps include Hénon maps[37], Sine boostable map[5], enhanced Hénon (E-Hénon) map[38], hidden NFIa map [39], and CFa map with curve fixed points (CFa)[40]. The same dimensional map include four 3D memristor-based maps that coupled the discrete memristor model with the Hénon map (3D-MH), the Duffing map (3D-MD), the Lozi map (3D-ML), and a 2D simple map (3D-MS), respectively[41]. Simulation experiments and statistical analysis have verified the satisfactory performance of the map (1). One can see that the map (1) constructed in this paper performs well on almost all four indicators, indicating the chaotic sequence generated by the map (1) has extremely high randomness and better unpredictability.

5.2 SE complexity

To investigate the impact of changes in two parameters on the complexity of the map (1), Fig. 14 plots the SE complexity maps of the parameters a and b within the range of $(-4, 4)$ and $(-50, 50)$. As can be observed from Fig. 14a, the complexity of the map (1) is at a low level when the absolute value of the parameters is small, as the absolute value of the parameters gradually increases, the SE complexity also increases and eventually stabilizing after reaching 0.95. In other words, the SE complexity of the map (1) is propor-

Table 3 Performance comparisons for chaotic sequences of some maps

| Chaotic maps	Parameters	Initial value	LE_{max}	SE	PE	CorDim
Hénon map [37]	(1.4,0.3)	(0,0)	0.4208	0.9276	4.2083	0.9107
Sine map [5]	(1.5,3.8)	(−2,1)	0.5316	0.9347	4.6675	0.9235
E-Hénon map [38]	(1,2)	(0,0.1)	1.0816	0.9502	4.7763	0.9502
NFIa map [39]	(−)	(0.93,−0.44)	0.0623	0.3076	2.3320	1.0293
CFa map [40]	(1.2,2)	(0.27,0.28)	0.1344	0.8328	3.5319	0.4512
3D-MH [41]	(0.3,0.1,0.7)	(0.5,0.5,0.1)	0.1862	0.6963	4.2847	1.9397
3D-MD [41]	(0.4,0.2,2)	(0.5,0.5,0.1)	0.3174	0.8763	4.0571	1.7963
3D-ML [41]	(0.3,0.1,1.8)	(0.5,0.5,0.1)	0.2633	0.6149	3.7383	1.8110
3D-MS [41]	(1.2,0.1,1.8)	(0.5,0.5,0.1)	0.2548	0.7196	3.7017	1.7803
Map (1)	(20,20)	(0.1,0.1,0.1)	1.8348	0.9508	4.7857	1.9062
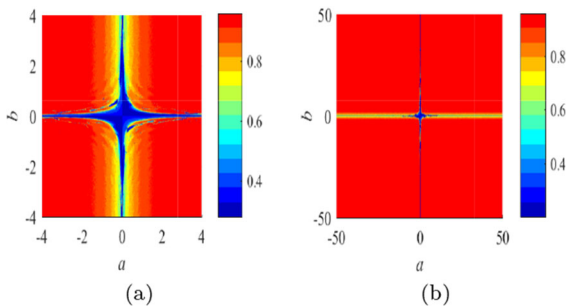
Fig. 14 **a** The SE complexity map on $a, b \in [−4, 4]$. **b** The SE complexity map on $a, b \in [−50, 50]$

tional to the absolute value of the parameters. Moreover, with an ultra-wide and continuous parameters range of higher complexity as shown in Fig. 14b, the map (1) has great advantages in secure communication and pseudo-random number generation.

5.3 NIST test

In order to test the randomness of the sequences generated by the map (1), this paper applies the National Institute of Standards and Technology (NIST) SP800-22 [42], which is a convincing comprehensive test standard and includes 15 sub-tests. Each sub-test is developed to find a group of non-random regions of binary sequences from various aspects. A significant level α in NIST SP800-22 is used to measure statistical error. In our experiment, the default significance level is selected as α=0.01. The length of each binary sequence should not be less than 10^6, and the number

of binary sequences should be greater than the reciprocal of the significance level, which is set to 120 in our experiment. Therefore, our experiment uses the map (1) to generate a set of 120 binary sequences with a length of 10^6, and tests the randomness of these binary sequences through NIST SP800-22. The test results can be judged from two aspects: the pass rate (Proportion) and P value. A P value greater than the significance level α indicates passing the test. The pass rate is measured through a confidence interval, which is calculated by

$$\left(1 - \alpha - 3\sqrt{\frac{\alpha(1 - \alpha)}{\beta}}, 1 - \alpha - 3\sqrt{\frac{\alpha(1 - \alpha)}{\beta}}\right)$$

where α the significance level, β is the number of test sequences. The confidence interval for this experiment was calculated to be (0.9628,1.0173).

Table 4 lists the test results, and it can be seen that the P values of all 15 tests are greater than 0.01, and the pass rates of all tests are within the confidence interval, which indicates that the sequence generated by the map (1) can pass all 15 tests (for some test items with multiple test results, only the smallest P value test result is listed in Table 4), and the sequences generated by the map (1) have higher randomness.

5.4 DSP implementation

The design of the hardware circuit is the key to the application of chaotic systems. Due to the multistability of the map (1), which is closely related to the

Table 4 NIST test results

No.	Test index	P value	Proportion
1	Frequency	0.383827	1.00
2	Block frequency	0.062821	0.97
3	Cumulative sums	0.657933	1.00
4	Runs	0.494392	0.98
5	Longest run	0.401199	0.99
6	Rank	0.699313	0.99
7	FFT	0.017912	0.99
8	Non-overlapping template	0.011791	1.00
9	Overlapping template	0.171867	1.00
10	Universal	0.474986	0.99
11	Approximate entropy	0.437274	0.99
12	Random excursions	0.023545	1.00
13	Random excursions variant	0.137282	1.00
14	Serial	0.834308	1.00
15	Linear complexity	0.779788	0.99
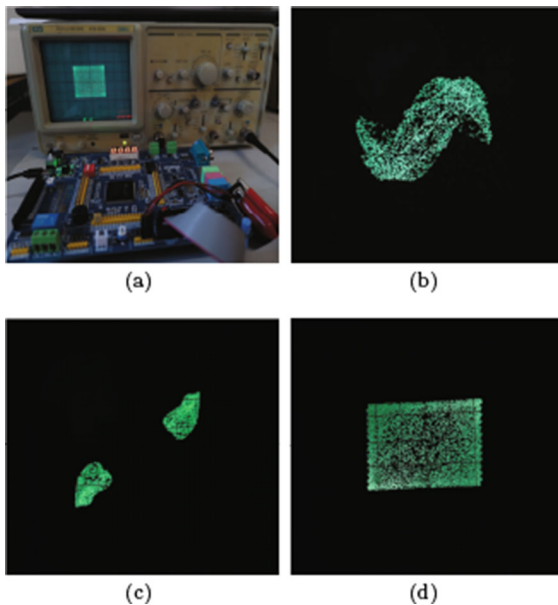
Fig. 15 DSP implementation: **a** Hardware diagram. **b** Chaotic attractor. **c** Symmetric chaotic attractor. **d** Hyperchaotic attractor

initial conditions, the stability and reliability of the hardware platform are required in practical projects. Besides, the discrete chaotic map can be naturally realized by digital circuits. Therefore, this paper utilizes the DSP hardware platform to implement the map (1). The hardware diagram is shown in Fig. 15a. In our experiment, we select a DSP hardware platform with the CPU TMS320F28335. We connect the simulator XDS100-V1 to the computer and utilize a 32-bit 4-channel DAC module with the chip of TLV5620 to output chaotic signals. The strange attractors are observed through the oscilloscope VOS-620B.

Fix initial value $(0.1, 0.1, 0.1)$. When parameters are set to $a = 1.57$ and $b = 1$, the chaotic attractor generated by the map (1) is shown in Fig. 15b. When $a = -5.2$ and $b = 0.5$, the symmetric chaotic attractor of (1) is shown in Fig. 15c. When $a = 40$ and $b = 30$, the hyperchaotic attractor of (1) is shown in Fig. 15d. The results in Fig. 15 achieve the consistency between theoretical simulation and hardware experiments, and also successfully verify the physical realizability and applicability of the map (1).

6 Conclusion

In this paper, we introduce a novel 3D non-degenerate hyperchaotic map. By using the modified perturbation method, we have proven that the map possesses at least one positive LE within an infinitely wide parameter range. The simulation results show that the

map exhibits rich dynamic behaviors highly related to the parameters, including an ultra-wide range of non-degenerate hyperchaotic parameters, enhanced ergodicity, antimonotonicity, and transient chaos. Moreover, the map exhibits various coexisting states, of particular significance is the phenomenon where symmetric chaotic attractors and quasi-periodic curves periodically switch, further enhancing the multistability. Furthermore, we have successfully achieved unidirectional polarity transformation of attractors, which, when combined with multistability, not only enhances the amplitude control of the chaotic sequence but also improves the performance of the new map in controlling and applying chaotic sequences.

Subsequently, our investigation focus on evaluating the effectiveness of the new map in generating random sequences and the feasibility of its potential applications in the fields of secure communication. To comprehensively assess the chaotic sequences generated by the map, we utilize multiple evaluation metrics, including SE, PE, and NIST test, among others, and the comparison results undoubtedly confirmed the high randomness and unpredictability of the generated chaotic sequences. In pursuit of practical validation, we utilized a DSP platform as our hardware experimental setup. Visualizing chaotic attractors via an oscilloscope provided dual validation: confirming numerical simulation results and highlighting the physical feasibility of the new map. Looking forward to future research, we anticipate delving deeper into the characteristics of the map, enabling broader applications, and making substantive contributions to the development of related fields.

Data availability The datasets generated during and/or analyzed during the current study are available from the corresponding author on reasonable request.

Declarations

Conflict of interest The authors declare that they have no conflict of interest.

References

1. Lorenz, E.N.: Deterministic nonperiodic flow. J. Atmos. Sci. **20**(2), 130–141 (1963)
2. Pan, J., Ding, Q., Du, B.: A new improved scheme of chaotic masking secure communication based on Lorenz system. Int. J. Bifurc. Chaos **22**(05), 1250125 (2012)
3. Bhatnagar, G., Wu, Q.J.: Chaos-based security solution for fingerprint data during communication and transmission. IEEE Trans. Instrum. Meas. **61**(4), 876–887 (2012)
4. Wang, X.Y., Li, Z.M.: A stream/block combination image encryption algorithm using logistic matrix to scramble. Int. J. Nonlinear Sci. Numer. Simul. **20**(2), 167–177 (2019)
5. Chen, S., Yu, S., Lü, J., Chen, G., He, J.: Design and fpga-based realization of a chaotic secure video communication system. IEEE Trans. Circuits Syst. Video Technol. **28**(9), 2359–2371 (2017)
6. Bao, H., Hua, Z., Wang, N., Zhu, L., Chen, M., Bao, B.: Initials-boosted coexisting chaos in a 2-d sine map and its hardware implementation. IEEE Trans. Ind. Inf. **17**(2), 1132–1140 (2020)
7. Yu, S., Jinhu, L., Li, C.: Some progresses of chaotic cipher and its applications in multimedia secure communications. J. Electron. Inf. Technol. **38**(3), 735–752 (2016)
8. Fan, C., Ding, Q., Tse, C.K.: Evaluating the randomness of chaotic binary sequences via a novel period detection algorithm. Int. J. Bifurc. Chaos **32**(5), 2250075 (2022)
9. Fan, C., Ding, Q.: Analysing the dynamics of digital chaotic maps via a new period search algorithm. Nonlinear Dyn. **97**, 831–841 (2019)
10. Liu, L., Miao, S.: Delay-introducing method to improve the dynamical degradation of a digital chaotic map. Inf. Sci. **396**, 1–13 (2017)
11. Luo, Y., Liu, Y., Liu, J., Tang, S., Harkin, J., Cao, Y.: Counteracting dynamical degradation of a class of digital chaotic systems via unscented kalman filter and perturbation. Inf. Sci. **556**, 49–66 (2021)
12. Chen, C., Sun, K., Peng, Y., Alamodi, A.O.: A novel control method to counteract the dynamical degradation of a digital chaotic sequence. Eur. Phys. J. Plus **134**, 1–16 (2019)
13. Fan, C., Ding, Q.: Analysis and resistance of dynamic degradation of digital chaos via functional graphs. Nonlinear Dyn. **103**(1), 1081–1097 (2021)
14. Heidari-Bateni, G., McGillem, C.D.: A chaotic direct-sequence spread-spectrum communication system. IEEE Trans. Commun. **42**(234), 1524–1527 (1994)
15. Alawida, M., Samsudin, A., Teh, J.S.: Enhanced digital chaotic maps based on bit reversal with applications in random bit generators. Inf. Sci. **512**, 1155–1169 (2020)
16. Wang, C., Fan, C., Ding, Q.: Constructing discrete chaotic systems with positive Lyapunov exponents. Int. J. Bifurc. Chaos **28**(07), 1850084 (2018)
17. Fan, C., Ding, Q.: A universal method for constructing non-degenerate hyperchaotic systems with any desired number of positive Lyapunov exponents. Chaos Solitons Fractals **161**, 112323 (2022)

18. Bao, H., Hua, Z., Li, H., Chen, M., Bao, B.: Discrete memristor hyperchaotic maps. IEEE Trans. Circuits Syst. I Regul. Pap. **68**(11), 4534–4544 (2021)

19. Chen, M., Luo, X., Suo, Y., Xu, Q., Wu, H.: Hidden extreme multistability and synchronicity of memristor-coupled non-autonomous memristive fitzhugh-nagumo models. Nonlinear Dyn. **111**(8), 7773–7788 (2023)

20. Zhang, L.P., Liu, Y., Wei, Z.C., Jiang, H.B., Lyu, W.P., Bi, Q.S.: Extremely hidden multi-stability in a class of two-dimensional maps with a cosine memristor. Chin. Phys. B **31**(10), 100503 (2022)

21. Shatnawi, M.T., Abbes, A., Ouannas, A., Batiha, I.M.: Hidden multistability of fractional discrete non-equilibrium point memristor based map. Phys. Scr. **98**(3), 035213 (2023)

22. Shen, C., Yu, S., Lü, J., Chen, G.: Designing hyperchaotic systems with any desired number of positive Lyapunov exponents via a simple model. IEEE Trans. Circuits Syst. I Regul. Pap. **61**(8), 2380–2389 (2014)

23. Shen, C., Yu, S., Lü, J., Chen, G.: A systematic methodology for constructing hyperchaotic systems with multiple positive Lyapunov exponents and circuit implementation. IEEE Trans. Circuits Syst. I Regul. Pap. **61**(3), 854–864 (2013)

24. Shen, C., Yu, S., Lü, J., Chen, G.: Constructing hyperchaotic systems at will. Int. J. Circuit Theory Appl. **43**(12), 2039–2056 (2015)

25. Huang, L., Liu, J., Xiang, J., Zhang, Z.: Design and analysis of a three-dimensional discrete memristive chaotic map with infinitely wide parameter range. Phys. Scr. **97**(6), 065210 (2022)

26. Dawson, S.P., Grebogi, C., Yorke, J.A., Kan, I., Koçak, H.: Antimonotonicity: inevitable reversals of period-doubling cascades. Phys. Lett. A **162**(3), 249–254 (1992)

27. Parlitz, U., Lauterborn, W.: Superstructure in the bifurcation set of the duffing equation. Phys. Lett. A **107**(8), 351–355 (1985)

28. Kocarev, L., Halle, K.S., Eckert, K., Chua, L.O.: Experimental observation of antimonotonicity in Chua's circuit. Int. J. Bifurc. Chaos **3**(04), 1051–1055 (1993)

29. Kengne, J., Negou, A.N., Tchiotsop, D.: Antimonotonicity, chaos and multiple attractors in a novel autonomous memristor-based jerk circuit. Nonlinear Dyn. **88**, 2589–2608 (2017)

30. Cassal-Quiroga, B., Gilardi-Velázquez, H., Campos-Cantón, E.: Multistability analysis of a piecewise map via bifurcations. Int. J. Bifurc. Chaos **32**(16), 2250241 (2022)

31. García-Martínez, M., Campos-Cantón, E.: Pseudo-random bit generator based on lag time series. Int. J. Mod. Phys. C **25**(04), 1350105 (2014)

32. Deng, Y., Li, Y.: A 2d hyperchaotic discrete memristive map and application in reservoir computing. IEEE Trans. Circuits Syst. II Express Briefs **69**(3), 1817–1821 (2021)

33. Ren, J., Ji'e, M., Xu, S., Yan, D., Duan, S., Wang, L.: RC-MHM: reservoir computing with a 2D memristive hyperchaotic map. Eur. Phys. J. Spec. Topics **232**(5), 663–671 (2023). https://doi.org/10.1140/epjs/s11734-023-00773-0

34. Bao, H., Chen, M., Wu, H., Bao, B.: Memristor initial-boosted coexisting plane bifurcations and its extreme multistability reconstitution in two-memristor-based dynamical system. Sci. China Technol. Sci. **63**(4), 603–613 (2020)

35. Bandt, C., Pompe, B.: Permutation entropy: a natural complexity measure for time series. Phys. Rev. Lett. **88**(17), 174102 (2002)

36. Theiler, J.: Efficient algorithm for estimating the correlation dimension from a set of discrete points. Phys. Rev. A **36**(9), 4456 (1987)

37. HENON, M.: A two-dimensonal mapping with a strange attractor. Commun. Math. Phys. **50**, 376–392 (1976)

38. Hua, Z., Zhou, Y., Bao, B.: Two-dimensional sine chaotification system with hardware implementation. IEEE Trans. Ind. Inf. **16**(2), 887–897 (2019)

39. Jiang, H., Liu, Y., Wei, Z., Zhang, L.: Hidden chaotic attractors in a class of two-dimensional maps. Nonlinear Dyn. **85**, 2719–2727 (2016)

40. Jiang, H., Liu, Y., Wei, Z., Zhang, L.: A new class of two-dimensional chaotic maps with closed curve fixed points. Int. J. Bifurc. Chaos **29**(07), 1950094 (2019)

41. Bao, H., Hua, Z., Li, H., Chen, M., Bao, B.: Memristor-based hyperchaotic maps and application in auxiliary classifier generative adversarial nets. IEEE Trans. Ind. Inf. **18**(8), 5297–5306 (2021)

42. Rukhin, A., Soto, J., Nechvatal, J., Smid, M., Barker, E.: A statistical test suite for random and pseudorandom number generators for cryptographic applications. Nist Special Publication (2001)